

See discussions, stats, and author profiles for this publication at: <https://www.researchgate.net/publication/274739183>

Fickian and Non-Fickian Diffusion in Heavy Oil + Light Hydrocarbon Mixtures

ARTICLE *in* ENERGY & FUELS · APRIL 2015

Impact Factor: 2.79 · DOI: 10.1021/ef502699c

CITATIONS

2

READS

31

2 AUTHORS, INCLUDING:



[Moien Alizadehgiashi](#)

University of Toronto

5 PUBLICATIONS 3 CITATIONS

[SEE PROFILE](#)

Fickian and Non-Fickian Diffusion in Heavy Oil + Light Hydrocarbon Mixtures

Moien Alizadehgiashi and John M. Shaw*

Department of Chemical and Materials Engineering, University of Alberta, Edmonton, Alberta T6G 2G6, Canada

S Supporting Information

ABSTRACT: Diffusive mass transfer is expected to play a key role in existing and proposed solvent-added processes for heavy oil production. Composition–distance profiles arising during free diffusion scale as a function of the joint variable (distance/time^{n_w}). Simple fluids are governed by Fickian diffusion, where $n_w = 0.5$. For nanostructured fluids, the value of n_w can be as low as $n_w = 0.25$, known as the single-file limit, but more typically, the value for the exponent falls between these two limits and is composition-dependent. In this work, five published data sets, comprising free diffusion composition profiles for Athabasca bitumen fractions and for Cold Lake bitumen + light hydrocarbons obtained using diverse apparatus, are probed from this perspective. Additional experimental results are provided for Athabasca bitumen + toluene mixtures over the temperature range of 273–313 K, and results from positive and negative control experiments for two well-defined mixtures—(0.25 mass fraction carbon nanotubes + polybutene) + toluene, and polybutene + toluene—are also provided. The value of n_w for the negative control experiment remains at 0.50 ± 0.05 over the entire composition range, and for the positive control experiment, the value drops to $n_w = 0.30 \pm 0.02$ at low toluene mass fraction. Although the quality of the diffusion profile data in the data sets analyzed is variable, the values of the exponent n_w are shown to be light-hydrocarbon-dependent and increase from $n_w \sim 0.25$ at low light-hydrocarbon mass fraction up to $n_w \sim 0.50$ at high light-hydrocarbon mass fraction. Secondary convective effects are also noted in free diffusion experiment outcomes at long times. The industrial applications of these findings are currently being evaluated, but it is clear that the time for light hydrocarbons to penetrate a fixed distance into nano- and micro-structured hydrocarbon resources is greater than the value anticipated for unstructured fluids.

INTRODUCTION

Athabasca Bitumen and other heavy hydrocarbon resources are high-mean-molar-mass and structured organic materials with complex phase behaviors at the nano- and micrometer length scales. Diffusion of light hydrocarbons and nonhydrocarbons in these resources is of significant interest as new production and refining concepts that envision, for example, addition of light hydrocarbons and nonhydrocarbons to reservoirs to enhance production have begun to emerge. Due to the phase behavior complexity and large difference in molecular properties of the hydrocarbon resources and the light hydrocarbon and nonhydrocarbons, mutual diffusion values per se, and perhaps more importantly the dominant mechanisms for diffusion are expected to vary with global composition.

The simplest analytic solution of the well-known one-dimensional differential form of Fick's free diffusion equation:^{1,2}

$$\frac{\partial c}{\partial t} = D \frac{\partial^2 c}{\partial x^2} \quad (1)$$

is normally expressed in dimensionless form as

$$c(x, t) = \frac{xc_0}{\sqrt{4\pi Dt}} e^{-x^2/4Dt} \quad (2)$$

where c is the mass or mole fraction of one of the fluid components, t is time, D is the mutual diffusion coefficient, and x is the spatial variable. In this solution, the mutual diffusion coefficient is assumed to be constant. If the mutual diffusion coefficient, D , is allowed to vary with composition, solutions of

eq 1 are more complex than eq 2, but time and distance variables appear jointly in each term with a fixed power relationship. Otherwise, mutual diffusion coefficients become a function of time at fixed composition. Such solutions are precluded by materials physics and chemistry. The power relationship, linked to the diffusion mechanism, is unrelated to the values of the mutual diffusion coefficient, or the dependence of the mutual diffusion coefficient on composition. The values and the composition dependence of the mutual diffusion coefficient determine the global shape of the composition profile but not whether or not the time and distance variables exhibit similarity. Thus, it is not necessary to solve for mutual diffusion coefficient values themselves in order to probe diffusion mechanisms from normalized composition profile data. This approach is commonly used to identify diffusion mechanisms.

For Fickian diffusion, composition–distance profiles obtained at different times can be superimposed if composition is expressed in terms of the joint variable:

$$\lambda = x/\sqrt{t} \quad (3)$$

This general and well-known result facilitates the evaluation of diffusion coefficients and is typically an excellent check on composition profile data quality where, for example, impacts of convection on results are readily detected. In structured fluids,

Received: December 4, 2014

Revised: February 6, 2015

Published: March 4, 2015

Table 1. Free Diffusion Composition Profile Data Sets Available in the Literature

mixture (number of composition profiles)	T (K)	experimental method	composition resolution (wt %)	C5 asphaltene (wt %)	ref
Athabasca bitumen + pentane (9)	293	vial + X-ray video imaging	0.3	18.6	11,12
Athabasca bitumen + toluene (5)	~293	microfluidic apparatus + visible light transmission imaging	0.15	18.6	13
Athabasca vacuum residue + pentane (5)	293	vial + X-ray video imaging	0.3	32	14
Athabasca atmospheric residue + pentane (5) ⁵	293	vial + X-ray video imaging	0.3	24 ^a	14
Cold Lake bitumen + heptane (5)	~ 293	vial placed in a CAT scanner	1	17.5 ^b	15

^aThis is an estimated value. ^bC7 asphaltene is 12 wt %¹⁵.

the concept of a space-time joint variable holds but the exponent becomes a variable and eq 3 becomes

$$\lambda_w = x/t^{n_w} \quad (4)$$

where the exponent n_w is a function of fluid structure. The minimum value for n_w was identified by Hodgkin and Keynes,³ who introduced the concept of the single-file diffusion limit in 1955. At the single-file limit, $n_w = 0.25$. This limit arises in highly structured fluids where molecules or particles cannot pass one another freely but must move through a medium or a constriction sequentially. This theoretical limit has been observed experimentally in diverse contexts over time.^{4–7} Thus, valid n_w values fall in the range 0.25 to 0.5. Intermediate values are observed experimentally because of mixed-mode diffusion. For example, in microchannels, Kamholz,⁸ and later Kamholz and Yager,⁹ showed that near the walls of a 10 μm wide microfluidic channel, $n_w = 1/3$ for pressure driven flow, on the basis of both theoretical calculations and experimental measurements. Ismagilov et al.¹⁰ also demonstrated experimentally that at steady state near the wall of pressure driven two phase laminar flow in a channel, transverse diffusion across the fluid–fluid interface scales with $n_w = 1/3$ as well. Careful experiments and data analysis are needed to ensure that individual mechanisms of mixed-mode diffusion can be discriminated, particularly as is the case in this work where variation of the dominant diffusion mechanism with global composition is expected.

From a theoretical perspective, it is easily shown that for integer values $i = 1, 2, 3, 4$, the general solution to the family of differential equations of the form:

$$\frac{\partial C}{\partial t} = D_i \frac{\partial^i C}{\partial x^i} \quad (5)$$

includes terms with the joint variable:

$$\lambda = x/t^{1/i} \quad (6)$$

irrespective of the details of the solution. Although the subject of a future work, from eqs 5 and 6, the values of $n_w = 1/2, 1/3$, and $1/4$ have clear roots both in mathematics and in observed physical phenomena. It is therefore possible to envision interpreting mixed-mode diffusion in structured media as a sum of Fickian and non-Fickian diffusive contributions.

To date, only the Fickian diffusion assumption, with either constant or variable mutual diffusion coefficient values, has been used to interpret free diffusion data for hydrocarbon resource + light hydrocarbon mixtures. Pertinent examples are noted in Table 1. In these published works,^{11–15} a lower density species diffuses and composition profiles are obtained as a function of time in viscous and hence quiescent media. Mutual diffusion coefficients were obtained in all of these examples by regressing composition versus distance profiles

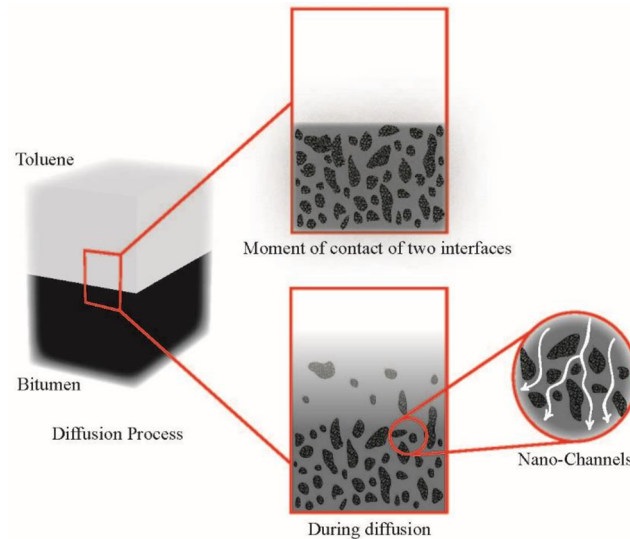


Figure 1. Simplified schematic for mutual diffusion between a light hydrocarbon + a nano/microstructured hydrocarbon resource sample.

Table 2. Properties of Athabasca Bitumen Used in This Study

property	value	ref
density (kg/m^3) @ 293 K	1026	16
complex viscosity ($\text{Pa}\cdot\text{s}$)		34
$\omega = 63 \text{ s}^{-1}$ and 0.3% shear strain		
@ 273 K	~90 000	
@ 298 K	~2000	
@ 313 K	~300	
SARA fractions (wt %)		
saturates	16.1	
aromatics	48.5	
resins	16.8	
asphaltenes (C5)	18.6	

assuming $n_w = 0.5$. It is worth noting that temperature was not controlled precisely for these measurements and that the Athabasca bitumen referred to in refs 11–13 are subsamples of the same master sample.

The assumption that $n_w = 0.5$ for heavy hydrocarbon resource + light hydrocarbon mixtures is revisited in the present work. These resources exhibit complex phase behaviors on their own^{16–19} and in mixtures with light hydrocarbons²⁰ and nonhydrocarbons.^{21,22} For example, phase diagrams for Athabasca Bitumen, Maya crude oil, and Safaniya vacuum residue have been prepared.^{16–19} These fluids comprise well-dispersed nanoscale asphaltene-rich phase domains and maltene-rich phase domains that undergo phase transitions in a largely independent manner.^{16–19} The asphaltene-rich phase

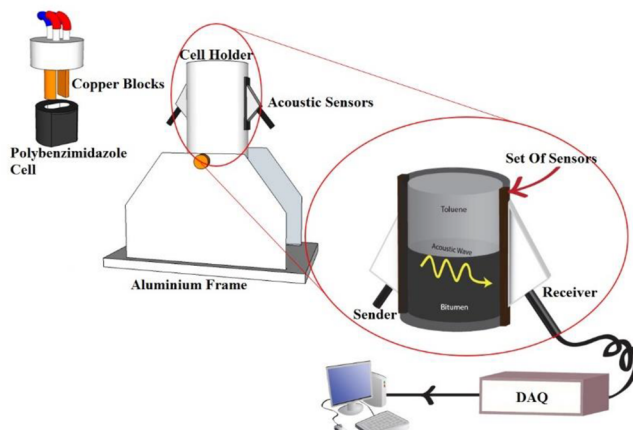


Figure 2. Schematic of the view cell and data acquisition system used for diffusion measurements showing the arrangement of the acoustic sensors as an inset.

domains comprise approximately 20 wt % of these fluids and are multiphase. Further, at temperatures below approximately 310 K, a fraction of the maltene-rich phase domains can also be multiphase-including solids. The presence of additional microscopic-length-scale liquid-crystal-rich domains further complicates the phase space.^{23,24} Finally, addition of light hydrocarbons to resource samples impacts their phase behavior both in time^{24,25} and with respect to the number and nature of phases.^{26–28} Although the exact structure and spatial distribution of phase domains in hydrocarbon resources such as Maya crude oil, Safaniya vacuum residue, and Athabasca bitumen are unknown, free diffusion between a light hydrocarbon and structured resource samples may be viewed from the perspective of a simple molecular fluid penetrating into a structured fluid comprising a broad range of nanoscopic and microscopic fluid-filled channels, as illustrated in Figure 1. In such complex fluids, Fickian and non-Fickian diffusive effects are expected to arise both with respect to composition, irrespective of time, and with respect to time at fixed composition as local phase behavior evolves.

The motivation to test this hypothesis arises from known aspects of the phase behavior of heavy oils, noted above, but it is also driven by industrial need. New processes for producing these resources are under development, which rely principally on diffusion for their successful application. Driven by joint desires to reduce the viscosity of the produced fluid, and hence to increase the rate of production, and to reduce the carbon dioxide emissions linked to current practice, interest in the development of new processes where light-hydrocarbons or nonhydrocarbons are injected into heavy oil and bitumen reservoirs^{29,30} has grown rapidly. If these processes are to be successful, detailed understanding of diffusion mechanisms and accurate diffusion rates for such mixtures are required. Consequently, this contribution comprises three parts. Composition profiles for the examples noted in Table 1 are evaluated to determine whether there is a detectable composition dependence for n_w as anticipated for structured + unstructured fluid mixtures. Further, as the nature and extent of the nano and microstructures present is expected to be temperature-dependent, additional composition profiles are obtained for Athabasca bitumen + toluene mixtures over a range of temperatures. Supporting measurements comprising positive and negative controls related to the determination of

the exponent n_w , based on the free diffusion method and equipment employed in the present study are also performed, and outcomes are discussed.

■ COMPOSITION PROFILE REGRESSION ALGORITHM TO DETERMINE LOCAL VALUES OF N_w AND THEIR UNCERTAINTY

This algorithm comprises three parts. First, local regression³¹ is used to smooth composition profile data so that comparisons at fixed composition can be made consistently. Following the local regression procedure, smoothing of weight fraction data, w_p , at a fixed elevation, x_p , is performed using a polynomial fit to (w_p, x_p) pairs in the neighborhood of the elevation of interest. The data point to be smoothed has the most influence on the fit, and data points outside the neighborhood have no influence on the fit. In this work, the neighborhood is defined as an interval of 0.05 mass fraction centered on the point of interest.

For free diffusion experiments, there is one elevation for which the composition is time invariant. This elevation is the origin of the coordinate system underlying the interpretation of free diffusion composition profiles. All composition profiles pass through this point, colloquially referred to as the crossover point. The elevation corresponding to the origin of the coordinate system is identified on the basis of smoothed composition profile data.

In the second step of the algorithm, sets of smoothed composition profiles are regressed to identify local values for n_w . Values and uncertainties related to two different regression approaches are presented. The local derivatives of the composition profiles, over a 0.05 mass fraction composition range, were fit by adjusting the value of n_w in eq 4, using least-squares regression to minimize the variation of the slope of the composition profiles within the composition interval of interest. Local integral fits to the composition profile data were also performed on the smoothed data. In this approach, local n_w values were obtained by minimizing the sum of absolute differences, σ_w , between individual λ_w values, defined in eq 4, that possess a common composition, w , obtained at 0.01 mass fraction increments and mean values, $\bar{\lambda}_w$, obtained over 0.05 mass fraction intervals:

$$\sigma_w = \frac{1}{j} \sum_{i=1}^j \left| 1 - \frac{\lambda_{w,i}}{\bar{\lambda}_w} \right| \quad (7)$$

For these fits the search limits for n_w were set as $0.15 < n_w < 0.75$ at a resolution of 0.025. Best-fit values were identified as the midpoint between adjacent values with the least error. These two regression approaches are complementary, even if they yield comparable values for n_w locally because of the composition dependence of their sensitivity to uncertainty in composition profile data. For example, at the crossover point, where composition is time invariant, regression of the slopes of the composition profiles can in principle provide good estimates for n_w ; however, irrespective of the value of n_w identified by minimizing the value of σ_w in eq 7, any value of n_w from negative to positive infinity is equally valid, and the best-fit value merely reflects experimental uncertainties related to composition, or distance. At compositions approaching $w = 0$ or 1, large uncertainties are anticipated for both approaches, but the values of n_w determined from derivative fits to the composition data are expected to be greater.

The third step of the algorithm comprises an assessment of the uncertainties of local n_w values. The range of uncertainty of

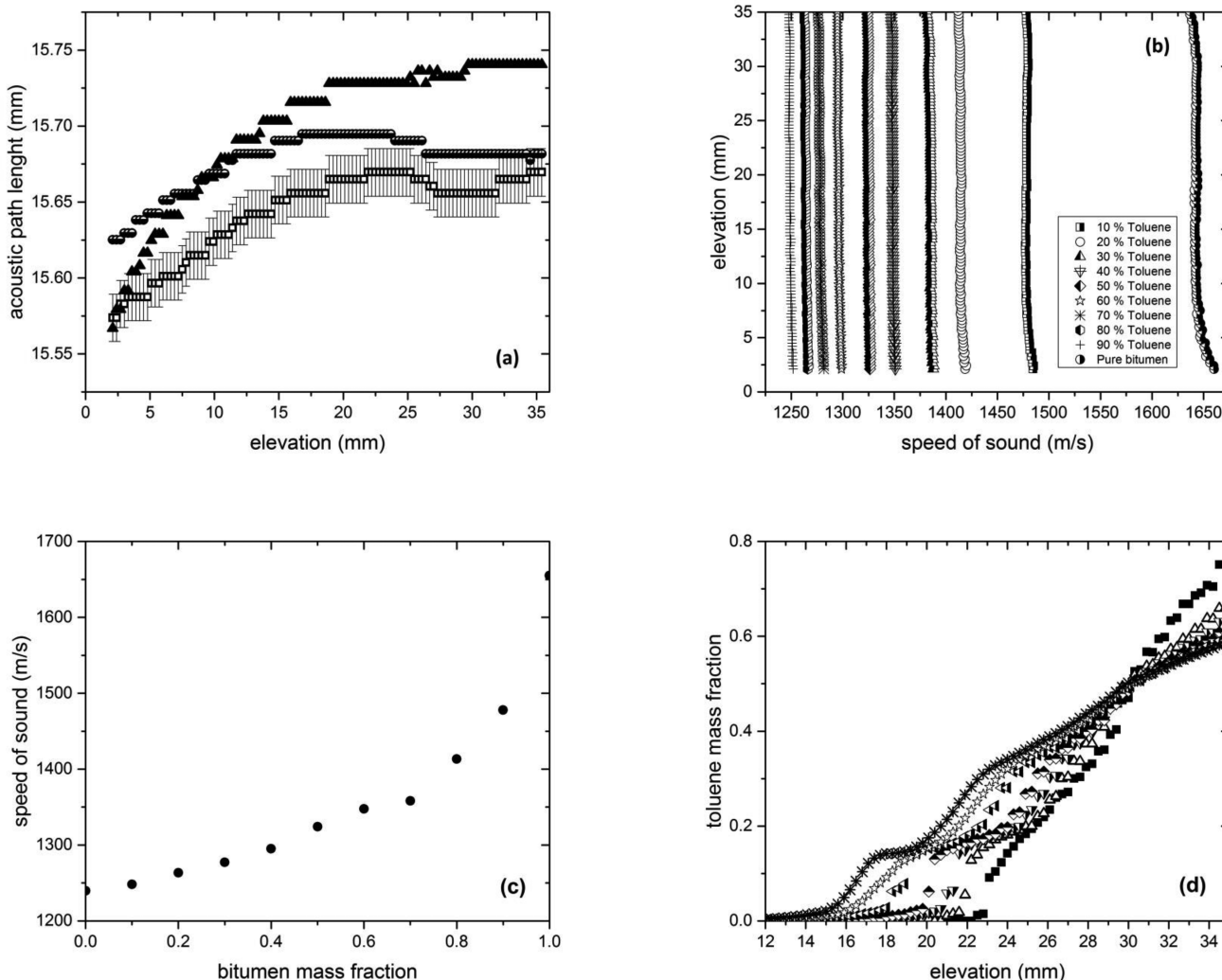


Figure 3. An illustration of the local composition calibration procedure: (a) acoustic path length determination at □, 273 K, ●, 298 K and ▲, 313 K; (b) speed of sound measurements for known mixtures of toluene + Athabasca bitumen at 313 K; (c) elevation-specific composition calibration curve for toluene + Athabasca bitumen mixtures at 313 K for the 20.1 mm elevation sensor; (d) composition profiles for toluene + Athabasca bitumen at 313 K. ■ 6 h, △ 12 h, ▽ 24 h, solid-base/left-facing ▽ 36 h, ☆ 48 h, * 60 h, + 72 h.

n_w values for a given composition and for specific data sets were established by determining the range of n_w values that allowed the composition profiles at all time steps to overlap within the composition measurement uncertainty. As a key objective of this study is to identify values for n_w , and it is not clear whether individual data sets are sufficiently accurate to do so, composition intervals where it was not possible to identify a range of n_w values that meet this criterion, are treated separately. Local values of n_w with an uncertainty that exceed 0.1 are excluded from the n_w determination irrespective of the mean. These criteria restrict the composition ranges for individual data sets from which n_w values can be extracted but provide reliable and objective criteria for their assessment. Composition profile smoothing is preferred and was selected for this work because it reduces the noise in digital signals and facilitates diffusion mechanism discrimination. Examples of n_w values and their uncertainties obtained from unsmoothed composition profile data using the same criteria are provided as supplemental data (Figures S1 and S2). n_w means are effectively the same, but the uncertainties are somewhat larger.

EXPERIMENTAL SECTION

Materials. Toluene (99%) was obtained from Fischer Scientific. Polybutene, supplied by Cannon Instruments as a Newtonian viscosity standard, has a viscosity of 1600 Pa·s and a density of 907 kg/m³ at 298 K. Carbon nanotubes, possessing an internal diameter of 5.5 nm, outer diameter of 6 to 9 nm and a length of 5 μm, were obtained from Aldrich. Athabasca Bitumen was provided from Syncrude Canada. Relevant properties of the Athabasca Bitumen sample are summarized in Table 2.

Apparatus and Procedure. In this work, composition profiles were determined by calibrating speed of sound values with composition and making use of an acoustic array data acquisition system attached to a thermostated cell. Local compositions were determined in a 4 cm tall cell using sealed sets of probes with elevation spacings of 600 μm. Measurements are averaged over a local length of 600 μm. Typical composition profiles comprise 50–70 composition–elevation pairs. The accuracy of the composition measurements is dictated by the reproducibility of local speed of sound values, better than ±3 m/s, and the difference in the speed of sound between the hydrocarbon resource sample and the light hydrocarbon, frequently more than 400 m/s. Thus, composition reproducibility uncertainties for composition are less than 0.01 (mass fraction basis).

A detailed description of the principles of measurement, the apparatus, the operating procedures, the data acquisition, and data

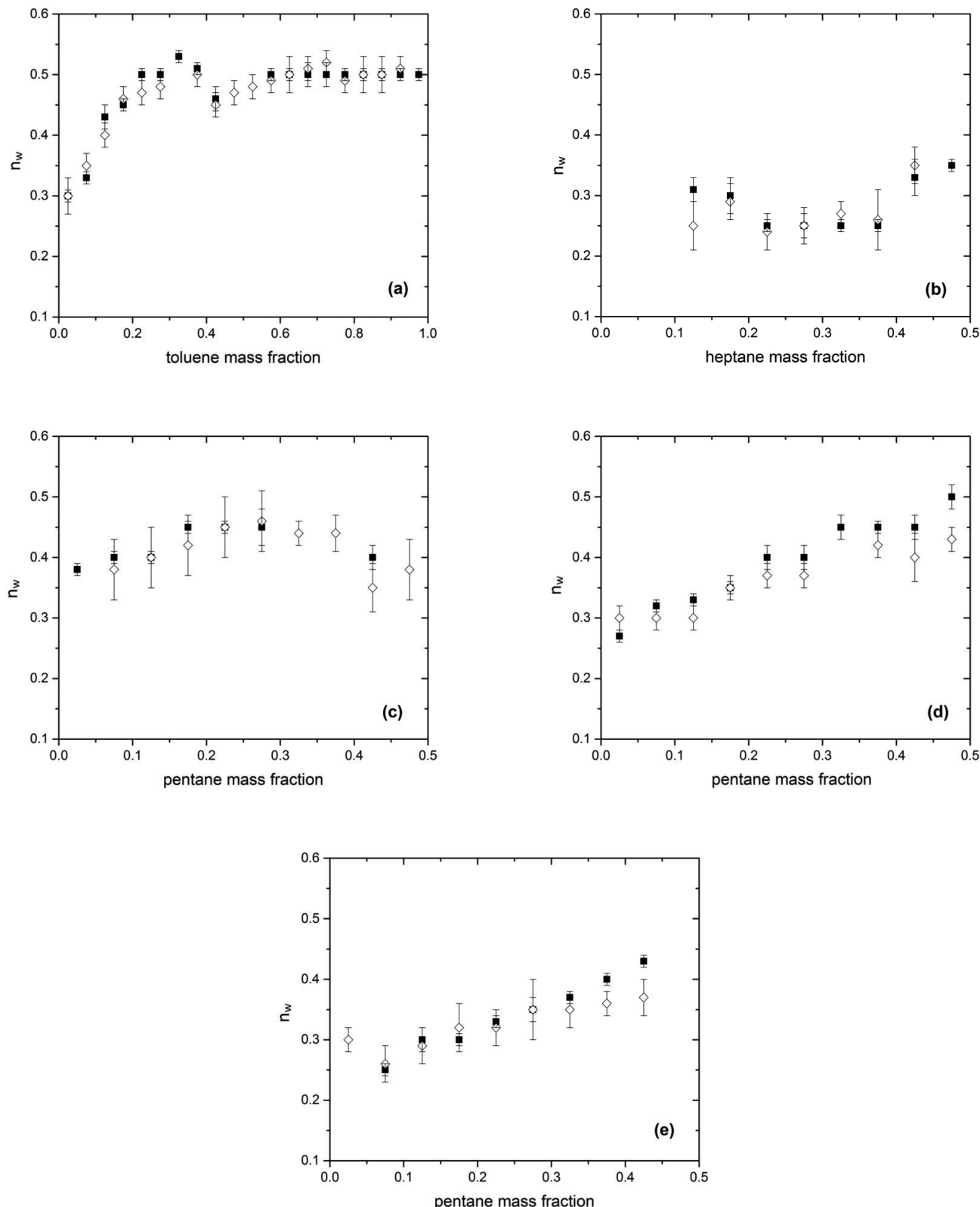


Figure 4. Local values of the time scaling exponent n_w and their uncertainty based on ■, minimizing σ_w and ◇, least-squares regression of slopes for the following: (a) Athabasca bitumen + toluene system;¹³ (b) Cold Lake bitumen + heptane;¹⁵ (c) Athabasca bitumen + pentane;¹¹ (d) Athabasca atmospheric residue + pentane;¹⁴ (e) Athabasca vacuum residue + pentane;¹⁴ at room temperature based on composition profiles obtained from the citations.

interpretation procedures are provided elsewhere.³² Only a brief overview and case specific details are presented here with reference to an apparatus schematic shown in Figure 2. Fluid samples were placed

in a polybenzimidazole cell within an aluminum frame. The cell was then sealed with an end-cap. The temperature was monitored and controlled using a thermistor probe, with an effective tolerance of ± 0.1

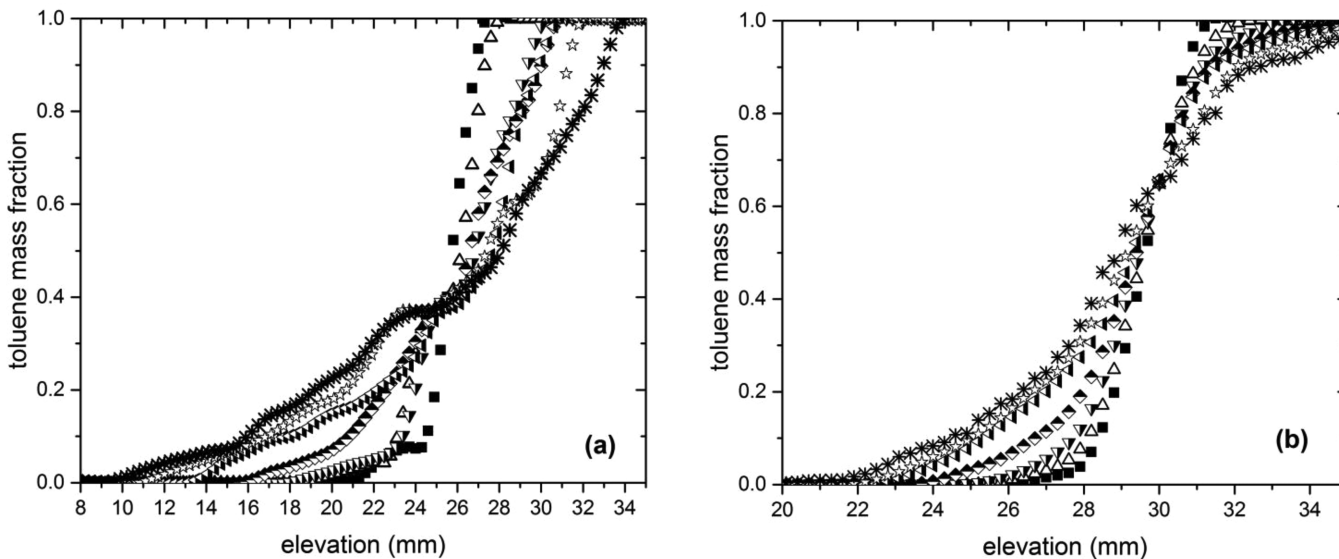


Figure 5. Raw composition vs elevation profiles for: (a) polybutene + toluene, and (b) toluene + (polybutene + 0.25 mass fraction carbon nanotubes) at 298 K. ■ 6 h, Δ 12 h, ▼ 24 h, tilted □ 36 h, solid-base/left-facing △ 48 h, ☆ 60 h, * 72 h.

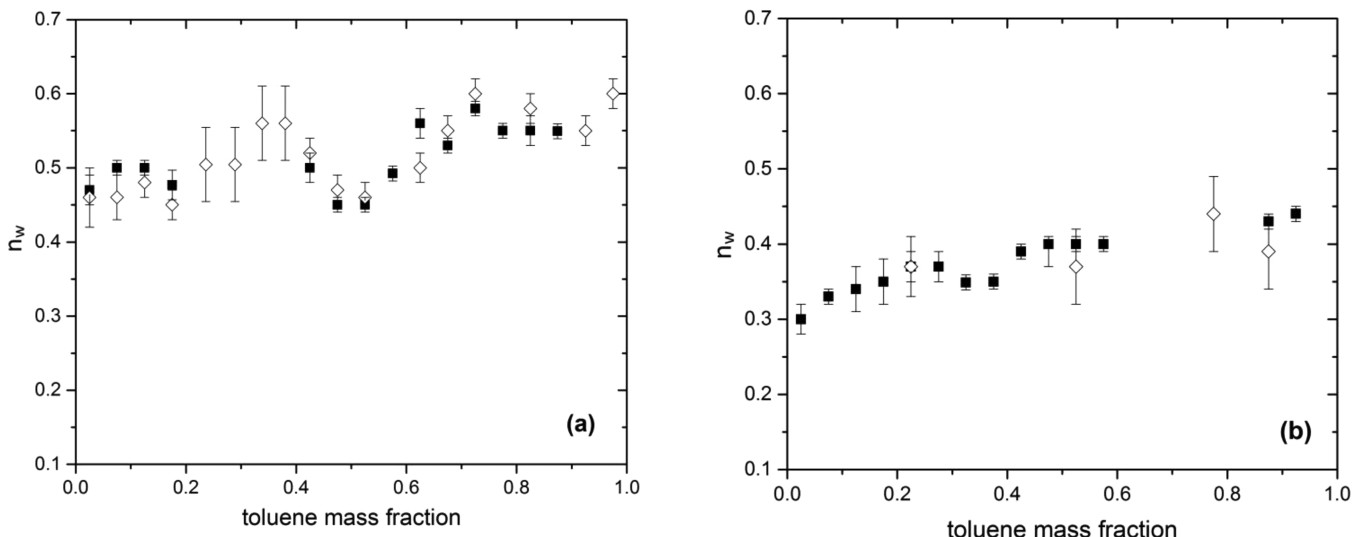


Figure 6. Local values of the time scaling exponent n_w and their uncertainty based on ■, minimizing σ_w and ◇, least-squares regression of slopes for: (a) polybutene + toluene and (b) (polybutene + 0.25 mass fraction carbon nano tubes) + toluene mixtures at 298 K.

K. An ethylene glycol + water mixture from a thermostated reservoir (Fisher Scientific Isotemp 3006D) was circulated through the two copper blocks that are attached to the end-cap and which fit within the cell cavity. The acoustic array sensors were screwed into place and coupled to the external walls of the cell using an acoustic coupling gel. The data acquisition hardware comprises a TomoScan Focus LT, and the data acquisition software comprises TomoView Software, both from Olympus NDT.

Speed of sound versus composition calibrations were assessed at each elevation for each pseudo binary mixture and at each temperature. The procedure is illustrated in Figure 3. First, path lengths as a function of elevation were determined based on time-of-flight measurements for toluene, which possesses a well-known speed of sound value as a function of temperature at atmospheric pressure [NIST]³³ (Figure 3a). Speeds of sound for mixtures of known composition, Athabasca bitumen + toluene in this example, Figure 3b, were then used to prepare composition calibration curves (Figure 3c) for each elevation so that mixtures of unknown composition could be interpolated. For this example, mixtures of known composition were prepared by combining Athabasca bitumen with toluene. At higher

mass fractions of toluene, a homogenizer (Fischer Scientific Analog Vortex Mixer) was used to homogenize mixtures. At lower toluene mass fractions, a bath sonicator operated at temperatures ranging 60 to 70 °C for at least 1 h was used to homogenize sealed vials containing mixtures. Composition profiles for Athabasca bitumen + toluene mixtures were obtained at 273, 298, and 313 K; local calibrations were obtained for each elevation at each of these temperatures. Calibrations for polybutene + toluene and polybutene + carbon nanotubes + toluene, at 298 K, were performed in a similar manner.

Athabasca bitumen is semisolid at room temperature, as noted in the introduction, and subsamples were heated to 353 K for 10 min so that they could be poured into the cell. The cell was then sealed and placed in an oven with air atmosphere at 353 K for 1 h before it was equilibrated in the frame at 323 K overnight to ensure the sample was uniformly distributed and free of gas bubbles. The bath temperature was then set to the desired temperature, and after thermal equilibrium was reached, toluene was injected into the upper portion of the cell using a syringe. As the cell and the copper blocks have a large thermal mass, and the temperature difference between the toluene and the set temperature of the cell is small, the duration of the thermal transient,

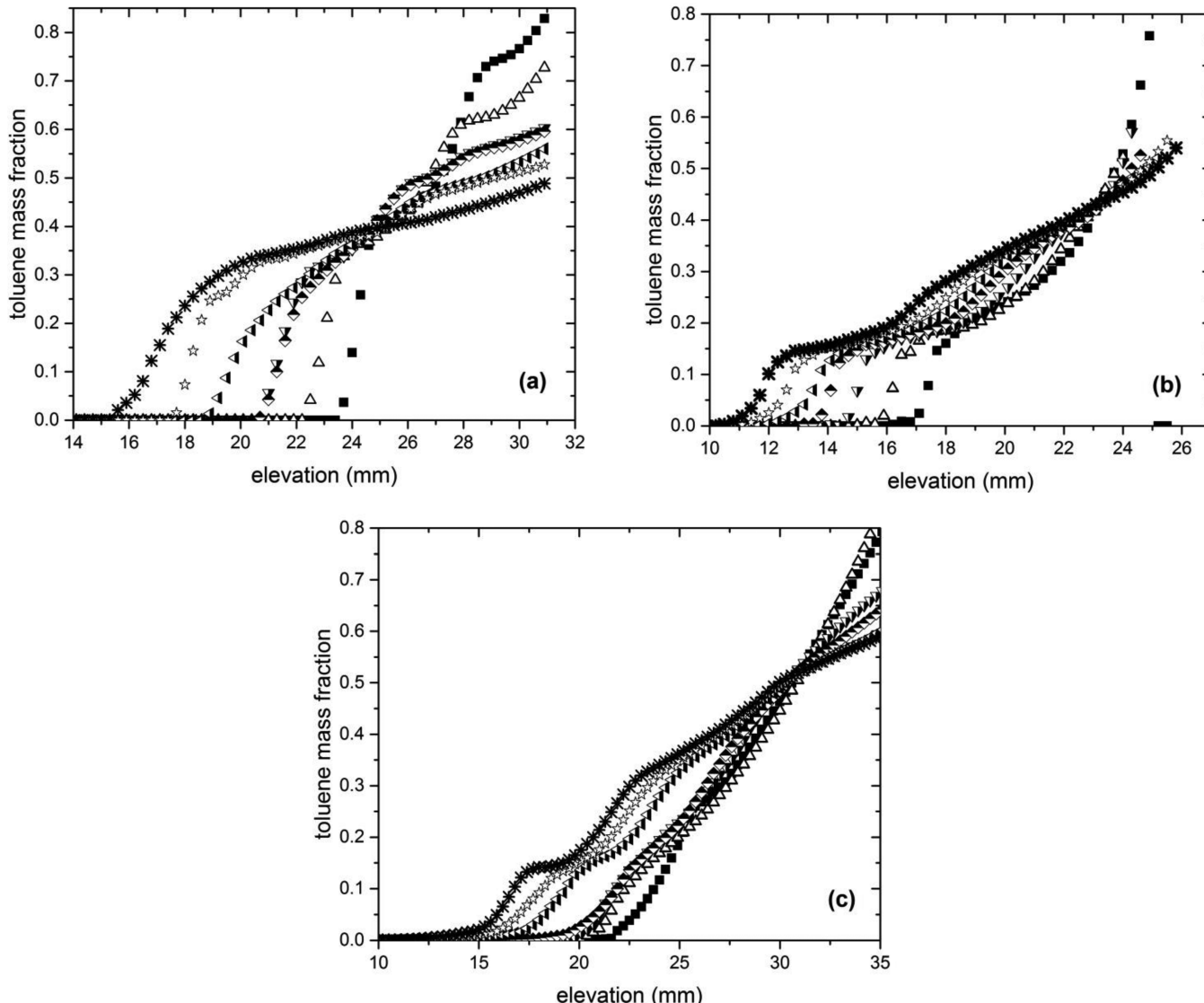


Figure 7. Smoothed composition profiles for Athabasca bitumen + toluene at the following: (a) 273 K, (b) 298 K and (c) 313 K. ■ 6 h, Δ 12 h, ▽ 24 h, tilted ■ 36 h, solid-base/left-facing △ 48 h, ☆ 60 h, * 72 h.

at less than ten seconds, is orders of magnitude smaller than the time scale of the diffusion measurements – hours. Composition profile evolution was assumed to begin at the time of injection.

Control experiments were performed at 298 K. Polybutene + toluene provided a negative control because polybutene + toluene mixtures comprise a single liquid phase. n_w is expected to be 0.5 over the entire composition range. To ensure that the high-viscosity polybutene was free of bubbles, it was placed in the polybenzimidazole cell and left in the oven at 353 K for 12 h. 25% carbon nanotubes + polybutene comprise a model structured fluid and for toluene + (carbon nanotubes + polybutene) pseudo binary mixtures values of n_w less than 0.5 are expected, particularly at low toluene mass fractions. The carbon nanotubes were combined with the polybutene at 353 K using a turbine impeller, described in detail elsewhere,¹⁴ and then treated in the same manner as the negative control sample. For these control experiments, care was also taken to ensure the absence of gas bubbles and well-defined horizontal interfaces at time zero. Polybutene was selected for control experiments because the viscosity of polybutene is comparable to the zero shear viscosity of Athabasca bitumen.

RESULTS AND DISCUSSION

Local Time-Invariant Values of n_w and Their Uncertainty Derived from Composition Profiles of Heavy Oil + Light Hydrocarbon Mixtures in the Literature. Local values of n_w , based on smoothed (Figure 4a–e) and unsmoothed (Figure S1) composition profile data and the criteria set out above, were obtained for the mixtures listed in Table 1. With reference to Figure 4, for all cases the exponent values are much less than 0.5 at low mass fractions of the light hydrocarbon. Convective or other effects, especially at longer times and at high light hydrocarbon mass fractions where the viscosity is orders of magnitude lower than the heavy hydrocarbon,^{35,36} impact the certainty of the exponent value determinations. The data obtained using the microfluidic free-diffusion apparatus, shown in Figure 4a, appear to be least impacted by this limitation due to the short time scale of the measurements. Composition profiles were obtained over a few minutes¹³ as opposed to multiple days for the other measurements. For the other data sets, Figure 4b–e, the composition ranges shown are restricted because it was not possible to fit all of the composition profiles to within

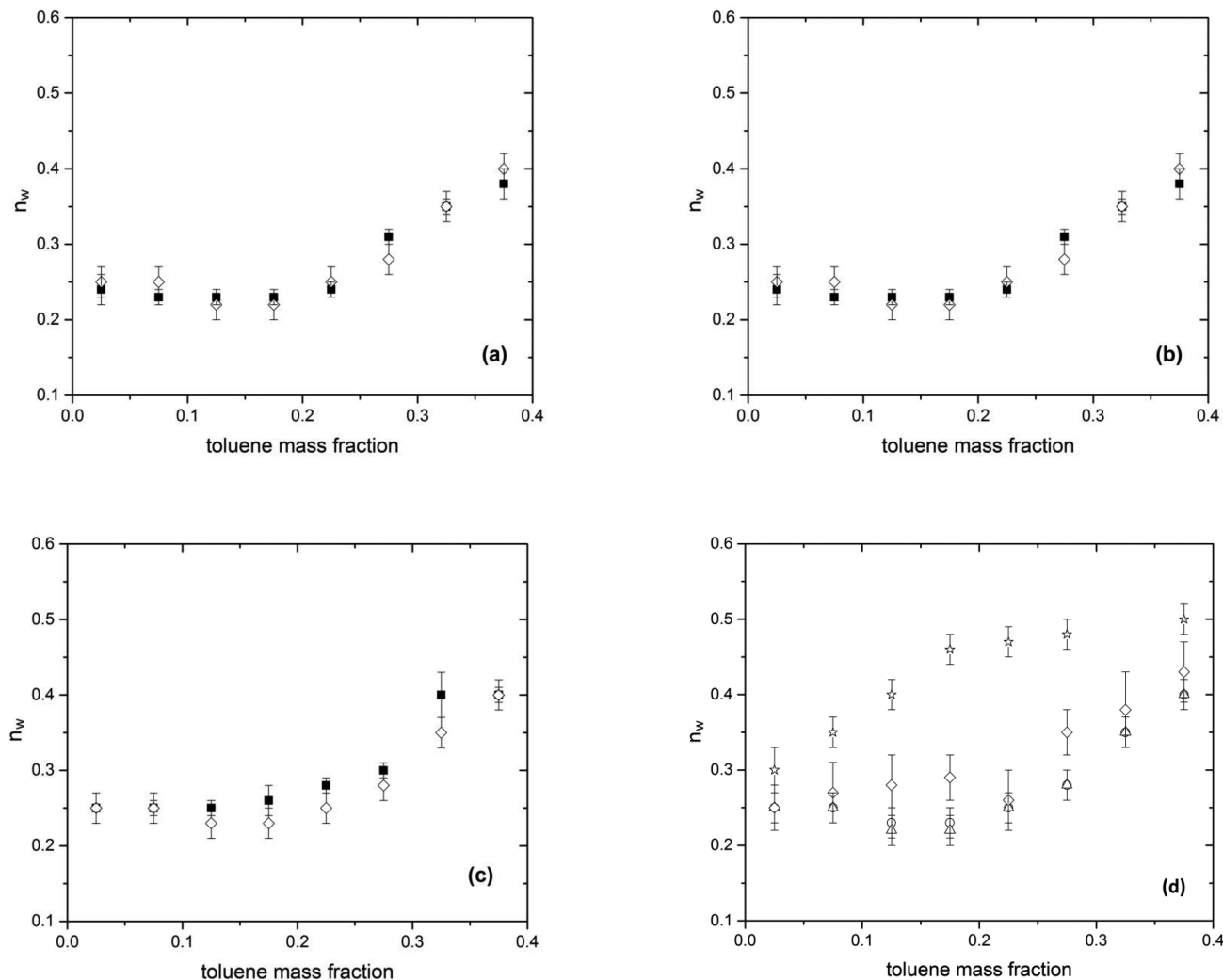


Figure 8. Time-scaling exponent (n_w) for Athabasca bitumen + toluene mixtures: (a) 273, (b) 298, and (c) 313 K based on ■, minimizing σ_w and ◊, least-squares regression of slopes. (d) Data set comparison for Athabasca bitumen + toluene mixtures based on minimizing σ_w : ☆, Fadaei et al.;¹³ ○, 273 K, Δ 298 K and ◇ 313 K.

experimental composition error simultaneously at higher light hydrocarbon mass fractions. All of the data sets deviate from Fickian behavior ($n_w = 1/2$). The mixtures reported in Figure 4a,b,d,e appear to be trending toward the single-file limit ($n_w = 1/4$) at low light hydrocarbon mass fraction. These same mixtures trend toward Fickian behavior at high light hydrocarbon mass fraction. The mixture reported in Figure 4 c, possesses an intermediate and constant value, $n_w \sim 0.4$, for the composition range $0 < w < 0.5$. The hypothesized non-Fickian behavior, particularly as the hydrocarbon resource axis is approached is clearly evident, in both the smoothed and unsmoothed data. This preliminary analysis sets the stage for careful experiments explicitly targeting the evaluation of n_w as a function of temperature and composition for heavy oil or bitumen + solvent mixtures.

Control Experiments. Toluene + polybutene mixtures should exhibit Fickian diffusion behavior irrespective of composition because both components are single phase and are fully miscible. Toluene + (0.25 mass fraction carbon nanotubes + polybutene) mixtures should exhibit non-Fickian diffusion behavior, especially at low toluene mass fraction. For these experiments, sets of composition calibration curves were prepared and used to interpret local speed of sound profiles and

to obtain raw composition versus elevation profiles, Figure 5a and 5b, respectively, following the procedure illustrated in Figure 3. These composition profiles were then processed in the same manner as the profiles obtained from the literature to derive local n_w values and their uncertainty. As is clear from Figure 6, toluene + polystyrene mixtures exhibit Fickian diffusion behavior, and n_w is well approximated as a composition invariant constant possessing a value of 0.50 ± 0.05 . For toluene + (0.25 mass fraction carbon nanotubes + polybutene), n_w possesses a marked composition dependence. n_w trends from ~ 0.3 , at low toluene mass fraction, toward $n_w = 0.5$ as the pure toluene axis is approached. Although n_w values determined by minimizing σ_w possess lower uncertainty than those obtained using least-squares regression of composition profile slopes, it is evident that the impact of the carbon nanotubes on diffusion persists with toluene mass fractions exceeding 0.90 based on either set of n_w values. The persistence of nanostucture is readily illustrated. If the density differences among constituents are ignored, then in the absence of toluene, the mean distance between adjacent carbon nanotubes at a mass fraction of 0.25 is approximately equal to the diameter of the nanotubes (5–7 nm). At a toluene mass fraction of 0.5, this mean distance becomes approximately 1.5 nanotube diameters

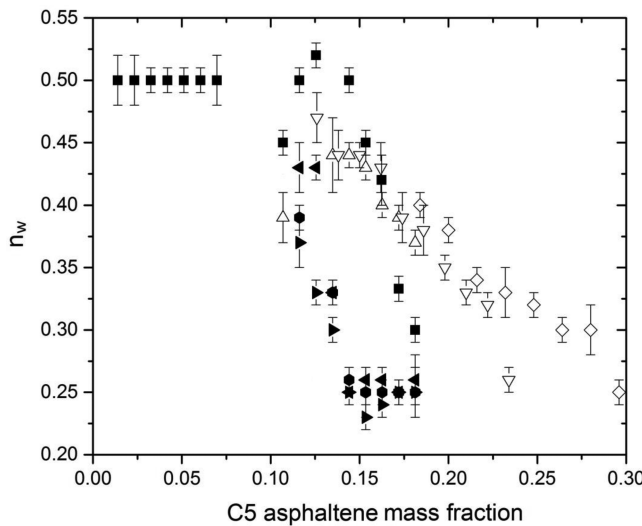


Figure 9. Values of n_w based on minimizing σ_w as a function of C5 asphaltene mass fraction in Athabasca bitumen-derived samples: Δ Athabasca bitumen + pentane;¹¹ ∇ Athabasca atmospheric residue + pentane,¹⁴ \diamond Athabasca vacuum residue + pentane;¹⁴ ■ Athabasca bitumen + toluene;¹³ Athabasca bitumen + toluene (this work), \blacklozenge 273 K, \blacktriangleright 298 K, and \blacktriangleleft 313 K.

(9–14 nm), and at a toluene mass fraction of 0.9, the mean distance is approximately 5 nanotube diameters (30–40 nm) and remains nanoscopic. It is only at toluene mass fractions approaching unity that the mean distances between nanoparticles become microscopic, much less macroscopic.

These control experiment data sets also serve two more general purposes. They illustrate that free diffusion measurements, made with the acoustic cell, provide reliable values for n_w with a resolution better than ± 0.05 for viscous fluid + light hydrocarbon mixtures over the entire composition range, even though the measurements take 2 or more days to complete. Convection even at high light hydrocarbon mass fractions has a minor impact on fluid transport over this long time interval. Consequently, variations in n_w values with time are interpretable. These results also illustrate that nanoparticles introduced into a fluid that exhibits Fickian diffusion behavior leads to non-Fickian diffusion behaviors that even for closely related fluids are observable and interpretable on the basis of free diffusion experiments.

Local Time-Invariant Values of n_w and Their Uncertainty Derived from Composition Profiles of Athabasca Bitumen + Toluene Mixtures. Composition profiles for Athabasca bitumen + toluene mixtures were obtained as illustrated in Figure 3 and are shown in Figure 7a–c for 273, 298, and 313 K. These profiles were then smoothed and processed as noted above. Local best-fit time-invariant values for n_w are shown for 273, 298, and 313 K in Figures 8a–c, respectively, over the composition interval 0–0.4 mass fraction toluene. n_w values and their uncertainties obtained from unsmoothed data for these cases are reported in the supplemental data (Figure S2). With reference to Figure 8, the n_w values approach the single-file limit ($n_w = 0.25$) at low toluene mass fraction at all three temperatures and possess a marked composition dependence, at all three temperatures, with a transition at ~ 0.25 mass fraction toluene. The temperature invariance of the composition dependence is readily seen in the comparison graphic, Figure 8d. Although the Athabasca bitumen sample was not expected to be at

equilibrium due to the metastability of liquid maltenes arising during the thermal treatment prior to experiments,¹⁶ temperature variation had been anticipated to play a more prominent role in the nature of the dominant diffusion mechanism(s). The absence of a temperature effect suggests that the nanostructure present in heated and then cooled Athabasca bitumen is essentially invariant over the temperature interval investigated. Regrettably, the nanostructure cannot be attributed to the maltenes-rich or the asphaltene-rich phases on the basis of these experimental results because neither phase undergoes a significant phase transition on reheating through the temperature range 273 to 313 K.¹⁶

Figure 8d provides a comparison between n_w outcomes from the current work and the work of Fadaei et al.¹³ for the same mixture. The two groups used subsamples from the same master sample, but variations in subsequent storage, handling, and sample pretreatment affect the details of the phase behavior¹⁶ of Athabasca bitumen, and the duration of the experiments differ by orders of magnitude. The two sets of n_w values are qualitatively similar and share common limits but possess quantitatively dissimilar composition dependencies over the composition interval 0–0.40 mass fraction toluene. A second point of contrast between the two sets of results arises at higher toluene mass fraction. It was not possible to identify low-uncertainty values for n_w in the current work, whereas from Fadaei et al.,¹³ a value of $n_w = 0.50$ obtains from 0.40 to 1.00 mass fraction toluene. In the absence of the negative control experiment, one would be tempted to attribute this to convection arising in the toluene rich fluid over time. However, the negative control experiment clearly illustrates that this is an inappropriate attribution. Further, the long-duration bitumen + solvent diffusion experiments from the literature share this same feature, and it would appear interpretable. Thus, kinetic effects linked to variation of nanostructure and microstructure with time at fixed composition require probing.

Impact of Asphaltene Mass Fraction and Solvent Choice on Local Time-Invariant n_w Values. With the large number of data points for Athabasca bitumen-related samples, it is possible to prepare a master plot showing values of n_w as a function of asphaltene mass fraction across the available studies. Sample pretreatments, storage, and handling differences remain uncontrolled variables in Figure 9, but it is possible to observe trends in the nature of the mutual diffusion behavior for Athabasca bitumen related samples + *n*-alkanes (open symbols) and toluene (closed symbols). As expected, Fickian diffusion is observed at low asphaltene mass fractions, and the single-file limit is approached at high asphaltene mass fraction. That the single-file limit is approached at a lower asphaltene mass fraction in toluene, than in *n*-alkanes, is superficially counterintuitive but readily explained. When aromatic solvents are added to heavy oils in general and to Athabasca bitumen fractions in particular, the size of nanoaggregates is largely unaffected, whereas addition of *n*-alkanes, even at low mass fraction, causes significant aggregate growth,^{37,38} prior to precipitation.³⁸ At high *n*-alkane mass fraction, asphaltenes in crude oils become microscopic and macroscopic. Thus, the spacing among structural elements grows from nanoscopic to microscopic and macroscopic with *n*-alkane addition. By contrast, with toluene addition, asphaltenes remain nanoscopic and the spacing among structural elements increases in a more limited manner with dilution and dissolution as more toluene is added. The positive control experiment, with carbon nanotubes, illustrates the significance of the impact of even small

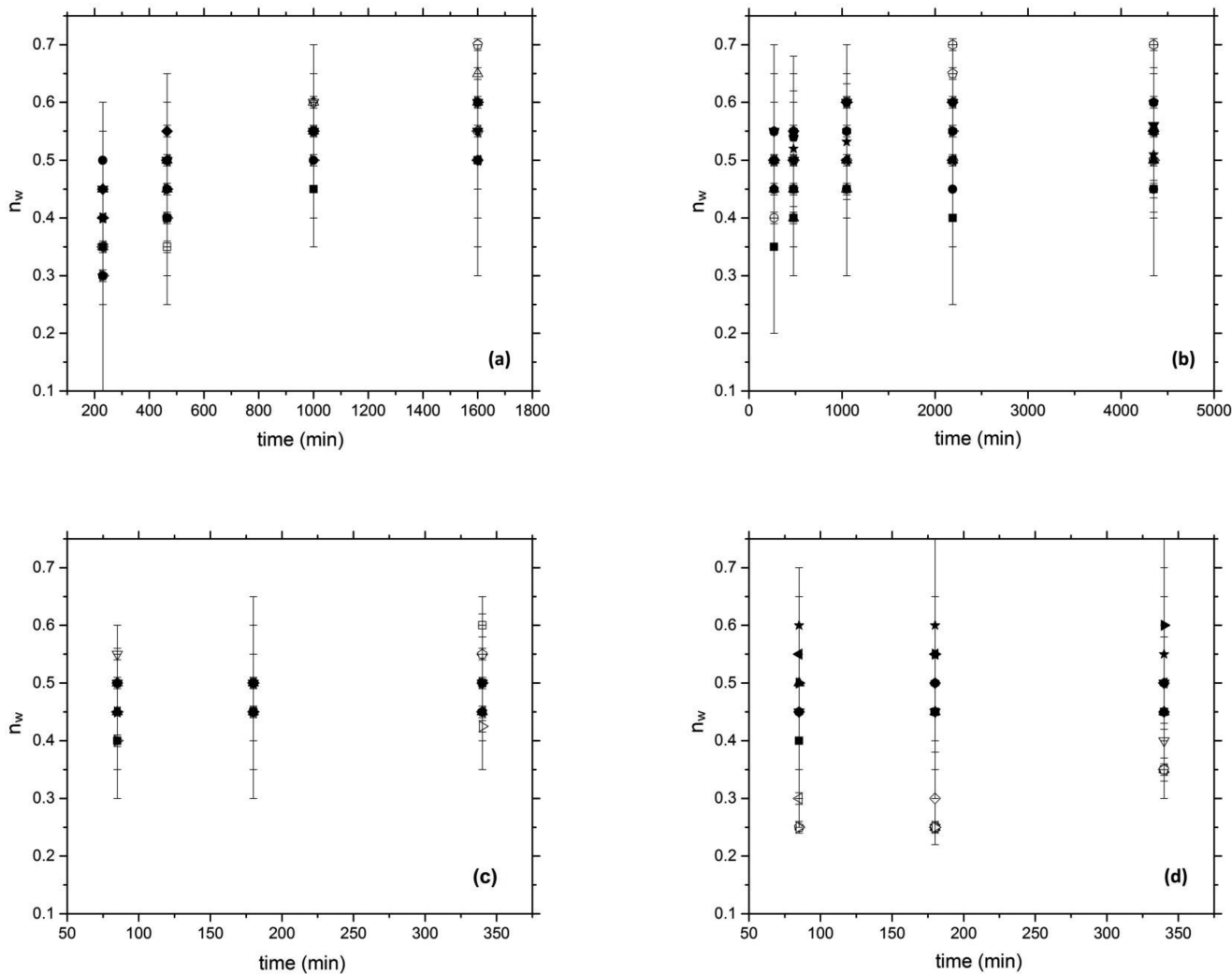


Figure 10. Temporal variation of n_w for (a) Cold Lake bitumen + heptane;¹⁵ (b) Athabasca bitumen + pentane;¹¹ (c) Athabasca atmospheric residue + pentane;¹⁴ (d) Athabasca vacuum residue + pentane.¹⁴ n_w values obtained by minimizing σ_w : □ 0.45 solvent mass fraction, ○ 0.5 solvent mass fraction, Δ 0.55 solvent mass fraction, ▽ 0.6 solvent mass fraction, ◇ 0.65 solvent mass fraction, left-facing ▲ 0.7 solvent mass fraction, ◇ 0.75 solvent mass fraction, ☆ 0.8 solvent mass fraction, △ 0.85 solvent mass fraction, left-facing ▲ 0.9 solvent mass fraction. n_w values obtained using least-squares regression of slopes: ■ 0.45 solvent mass fraction, ● 0.5 solvent mass fraction, ▲ 0.55 solvent mass fraction, ▽ 0.6 solvent mass fraction, ♦ 0.65 solvent mass fraction, ◀ 0.7 solvent mass fraction, ▶ 0.75 solvent mass fraction, ◆ 0.8 solvent mass fraction, ★ 0.85 solvent mass fraction.

volume fractions of nanostructured elements on diffusive mass transfer. Thus, n -alkanes, or other similar solvents, appear to be preferred penetrants for heavy oils and bitumen from a diffusion perspective, as suggested by the results in Figure 9. Larger n_w values imply faster penetration.

Temporal Variation of n_w Values at High Solvent Mass Fraction

Temporal variation of n_w values arising at high solvent mass fraction in heavy oil + light hydrocarbon mutual diffusion experiments, may arise from temporal changes in fluid physics and chemistry or as a consequence of convective and other fluid mechanic effects in systems with flow. This issue is explored in Figure 10, for data sets from the literature, and in Figure 11, for Athabasca bitumen + toluene mixtures studied in this work. For these evaluations, two consecutive composition profiles in the composition profile time series were fit at 0.05 mass fraction intervals, outside the composition range where low-uncertainty time-invariant values were obtained. The n_w values at fixed composition reported in Figures 10 and 11 possess high uncertainties and do not vary significantly with

time. The best-fit value data sets as a whole clearly do drift to higher values with time for Cold Lake bitumen + heptane (Figure 10a) and for Athabasca bitumen + pentane (Figure 10b). Beyond 1500 min, there is evidence for convection at high pentane/heptane mass fraction as n_w values as large as 0.7 are derived from the data. Changes in those parts of the composition profiles cannot be interpreted as reflecting diffusive mass transfer alone and should be excluded from mutual diffusion coefficient evaluation calculations. For Athabasca atmospheric and vacuum residue + pentane (Figure 10c,d), which cover a narrower range of compositions, there is no apparent systematic variation with time within the uncertainty of the data. Possible impacts of convection cannot be detected. For the measurements reported in this work, Figure 11a–c, the outcome is comparable. The individual values for n_w possess significant uncertainty. The best-fit n_w values drift higher as a collective but remain largely within the $0.45 < n_w < 0.55$ range. Consequently, the possible impact of convection is approaching the detection limit. Overall, there is

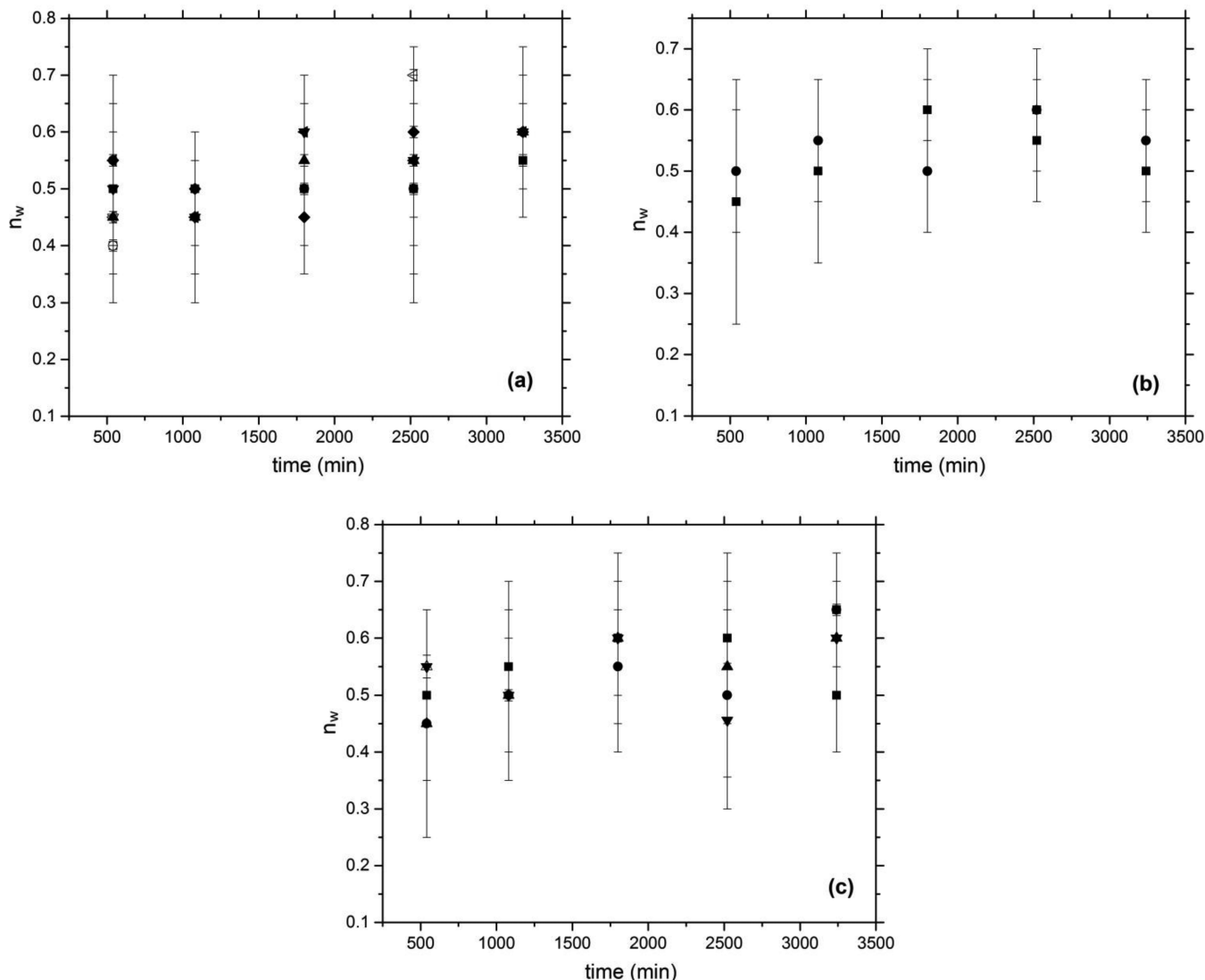


Figure 11. Temporal variation of n_w values for Athabasca bitumen + toluene (a) 273 K (b) 298 K (c) 313 K. n_w values obtained by minimizing σ_w : □ 0.45 solvent mass fraction, ○ 0.5 solvent mass fraction, Δ 0.55 solvent mass fraction, ▽ 0.6 solvent mass fraction, ◇ 0.65 solvent mass fraction, left-facing ▲ 0.7 solvent mass fraction, □ 0.75 solvent mass fraction, ★ 0.8 solvent mass fraction. n_w values obtained from least-squares regression of slopes: ■ 0.45 solvent mass fraction, ● 0.5 solvent mass fraction, ▲ 0.55 solvent mass fraction, ▼ 0.6 solvent mass fraction, ◁ 0.65 solvent mass fraction, ▲ 0.7 solvent mass fraction, ▶ 0.75 solvent mass fraction, ◆ 0.8 solvent mass fraction.

no evidence for a composition linked temporal dependence for n_w across all of the data sets, and from the perspective of minimizing the impact of convective effects at high penetrant mass fraction, the microfluidics method is clearly preferred.

CONCLUSIONS

Unambiguous identification of Fickian and non-Fickian diffusion mechanisms in sets of free diffusion composition profile data imposes significant constraints on the quality of time, distance and composition measurements, and careful data processing. Control experiments and two composition profile fitting techniques applied to polybutene + toluene and polybutene + toluene + carbon nanotube showed that free diffusion is in principle an appropriate basis for discriminating diffusion behaviors of closely related mixtures and that convective effects play a secondary role even in mixtures with low viscosity. Convective effects do not interfere with the identification the principal diffusion mechanisms from composition profiles in the literature or obtained in this

work. Diffusion at low penetrant mass fractions in nano- and microstructured hydrocarbon resources, such as Athabasca and Cold Lake bitumen, is shown to be governed by the single-file limit, a non-Fickian diffusion mechanism, whereas at high penetrant mass fraction, diffusion is shown to be governed by Fickian diffusion. The transition from non-Fickian to Fickian diffusion as penetrant is added is shown to be penetrant-dependent. The difference in the behavior of *n*-alkanes and toluene as penetrants is attributed to their respective impacts on asphaltene nanostructure. *N*-alkanes cause the asphaltene fraction to aggregate at low mass fraction and to form micro- or macroscale objects at high mass fraction. In toluene, the asphaltenes remain nanodispersed. The mixture remains nanostructured at higher penetrant mass fractions in toluene than in *n*-alkanes, and this delays the gradual transition from non-Fickian to Fickian diffusion. Mixed Fickian and single-file diffusion modes of diffusion coexist at intermediate compositions. The impacts of these findings on mutual diffusion coefficient value evaluation and on industrial applications are

currently being explored. However, it is clear that the time for light hydrocarbons to penetrate a fixed distance into nano- and microstructured hydrocarbon resources is significantly greater than anticipated based on Fickian diffusion.

■ ASSOCIATED CONTENT

S Supporting Information

Example n_w data sets obtained from unsmoothed composition profiles corresponding to the cases presented in Figure 4a–e and Figure 8a–c are provided as Figures S1 a–e and Figure S2 a–c, respectively. This material is available free of charge via the Internet at <http://pubs.acs.org>.

■ AUTHOR INFORMATION

Corresponding Author

*E-mail jmshaw@ualberta.ca. Phone: +1 780 492 8236.

Notes

The authors declare no competing financial interest.

■ ACKNOWLEDGMENTS

The authors thank Professors Kantzas (University of Calgary) and Sinton (University of Toronto), for making their composition profiles available; Mr. Robert Stewart, Dr. Mohammad Javad Amani, Dr. Marc Cassiede and Ms Mildred Becerra, for their help in the laboratory; and Mr. Saman Jahani for help with graphics. The authors gratefully acknowledge financial support from the sponsors of the NSERC Industrial Research Chair in Petroleum Thermodynamics: Natural Sciences and Engineering Research Council of Canada (NSERC), Alberta Innovates, ConocoPhillips Canada Resources Corp., Shell Canada Ltd., Nexen Energy ULC, Virtual Materials Group (VMG), Total E&P Canada Ltd.

■ REFERENCES

- Bird, R.B.; Stewart, W.E.; Lightfoot, E.N. *Transport Phenomena*; John Wiley & Sons: New York, 2007.
- Crank, J. *The mathematics of diffusion*; Clarendon Press: Oxford, U.K., 1975.
- Hodgkin, A. L.; Keynes, R. D. The potassium permeability of a giant nerve fibre. *J. Physiol.* **1955**, *128*, 61–88.
- Wei, Q.-H.; Bechinger, C.; Leiderer, P. Single-File Diffusion of Colloids in One-Dimensional Channels. *Science* **2000**, *287*, 625–627.
- Lin, B.; Meron, M.; Cui, B.; Rice, S. A.; Diamant, H. From Random Walk to Single-File Diffusion. *Phys. Rev. Lett.* **2005**, *94*, 216001.
- Mason, T. G. Osmotically driven shape-dependent colloidal separations. *Phys. Rev. E* **2002**, *66*, 060402.
- Meersmann, T.; Logan, J. W.; Simonutti, R.; Caldarelli, S.; Comotti, A.; Sozzani, P.; et al. Exploring Single-File Diffusion in One-Dimensional Nanochannels by Laser-Polarized ^{129}Xe NMR Spectroscopy. *J. Phys. Chem. A* **2000**, *104*, 11665–11670.
- Kamholz, A. E.; Weigl, B. H.; Finlayson, B. A.; Yager, P. Quantitative Analysis of Molecular Interaction in a Microfluidic Channel: The T-Sensor. *Anal. Chem.* **1999**, *71*, 5340–5347.
- Kamholz, A. E.; Yager, P. Molecular diffusive scaling laws in pressure-driven microfluidic channels: deviation from one-dimensional Einstein approximations. *Sens. Actuators, B* **2002**, *82*, 117–121.
- Ismagilov, R. F.; Stroock, A. D.; Kenis, P. J. A.; Whitesides, G.; Stone, H. A. Experimental and theoretical scaling laws for transverse diffusive broadening in two-phase laminar flows in microchannels. *Appl. Phys. Lett.* **2000**, *76*, 2376–2378.
- Zhang, X.; Fulem, M.; Shaw, J. M. Liquid-Phase Mutual Diffusion Coefficients for Athabasca Bitumen + Pentane Mixtures. *J. Chem. Eng. Data* **2007**, *52*, 691–694.
- Zhang, X.; Shaw, J. M. Liquid-phase Mutual Diffusion Coefficients for Heavy Oil + Light Hydrocarbon Mixtures. *Pet. Sci. Technol.* **2007**, *25*, 773–790.
- Fadaei, H.; Shaw, J. M.; Sinton, D. Bitumen–Toluene Mutual Diffusion Coefficients Using Microfluidics. *Energy Fuels* **2013**, *27*, 2042–2048.
- Sadighian, A.; Becerra, M.; Bazyleva, A.; Shaw, J. M. Forced and Diffusive Mass Transfer between Pentane and Athabasca Bitumen Fractions. *Energy Fuels* **2011**, *25*, 782–790.
- Wen, Y. W.; Kantzas, A. Monitoring Bitumen–Solvent Interactions with Low-Field Nuclear Magnetic Resonance and X-ray Computer-Assisted Tomography†. *Energy Fuels* **2005**, *19*, 1319–1326.
- Bazyleva, A.; Fulem, M.; Becerra, M.; Zhao, B.; Shaw, J. M. Phase Behavior of Athabasca Bitumen. *J. Chem. Eng. Data* **2011**, *56*, 3242–3253.
- Fulem, M.; Becerra, M.; Hasan, M. D. A.; Zhao, B.; Shaw, J. M. Phase behaviour of Maya crude oil based on calorimetry and rheometry. *Fluid Phase Equilib.* **2008**, *272*, 32–41.
- Zhao, B.; Shaw, J. M. Composition and Size Distribution of Coherent Nanostructures in Athabasca Bitumen and Maya Crude Oil. *Energy Fuels* **2007**, *21*, 2795–2804.
- Bazyleva, A.; Becerra, M.; Stratichuk-Dear, D.; Shaw, J. M. Phase behavior of Safaniya vacuum residue. *Fluid Phase Equilib.* **2014**, *380*, 28–38.
- Díaz, O. C.; Modaresghazani, J.; Satyro, M. A.; Yarranton, H. W. Modeling the phase behavior of heavy oil and solvent mixtures. *Fluid Phase Equilib.* **2011**, *304*, 74–85.
- Amani, M. J.; Gray, M. R.; Shaw, J. M. The phase behavior of Athabasca bitumen + toluene + water ternary mixtures. *Fluid Phase Equilib.* **2014**, *370*, 75–84.
- Amani, M. J.; Gray, M. R.; Shaw, J. M. Phase behavior of Athabasca bitumen + water mixtures at high temperature and pressure. *J. Supercrit. Fluids* **2013**, *77*, 142–152.
- Bagheri, S. R.; Bazyleva, A.; Gray, M. R.; McCaffrey, W. C.; Shaw, J. M. Observation of Liquid Crystals in Heavy Petroleum Fractions. *Energy Fuels* **2010**, *24*, 4327–4332.
- Bagheri, S. R.; Masik, B.; Arboleda, P.; Wen, Q.; Michaelian, K. H.; Shaw, J. M. Physical Properties of Liquid Crystals in Athabasca Bitumen Fractions. *Energy Fuels* **2012**, *26*, 4978–4987.
- Nikooyeh, K.; Bagheri, S. R.; Shaw, J. M. Interactions Between Athabasca Pentane Asphaltenes and n-Alkanes at Low Concentrations. *Energy Fuels* **2012**, *26*, 1756–1766.
- Saber, N.; Zhang, X.; Zou, X.-Y.; Shaw, J. M. Simulation of the phase behaviour of Athabasca vacuum residue + n-alkane mixtures. *Fluid Phase Equilib.* **2012**, *313*, 25–31.
- Saber, N.; Shaw, J. M. On the phase behaviour of Athabasca vacuum residue + n-decane. *Fluid Phase Equilib.* **2011**, *302*, 254–259.
- Saber, N.; Shaw, J. M. Toward multiphase equilibrium prediction for ill-defined asymmetric hydrocarbon mixtures. *Fluid Phase Equilib.* **2009**, *285*, 73–82.
- Stewart, R.; Wood, C. V.; Murowchuk, S. J.; Shaw, J. M. Phase Order Inversion During Heavy Oil and Bitumen Production with Solvent Addition. *Energy Fuels* **2014**, *28*, 4835–4848.
- Shah, A.; Fishwick, R.; Wood, J.; Leeke, G.; Rigby, S.; Greaves, M. A review of novel techniques for heavy oil and bitumen extraction and upgrading. *Energy Environ. Sci.* **2010**, *3*, 700–714.
- Cleveland, W. S. Robust Locally Weighted Regression and Smoothing Scatterplots. *J. Am. Stat. Assoc.* **1979**, *74*, 829–836.
- Khammar, M.; Shaw, J. M. Phase behaviour and phase separation kinetics measurement using acoustic arrays. *Rev. Sci. Instrum.* **2011**, *82*, 104902.
- NIST Chemistry WebBook. <http://webbook.nist.gov/chemistry/>
- Bazyleva, A. B.; Hasan, M. A.; Fulem, M.; Becerra, M.; Shaw, J. M. Bitumen and Heavy Oil Rheological Properties: Reconciliation with Viscosity Measurements. *J. Chem. Eng. Data* **2010**, *55*, 1389–1397.

(35) Guan, J. G.; Kariznovi, M.; Nourozieh, H.; Abedi, J. Density and Viscosity for Mixtures of Athabasca Bitumen and Aromatic Solvents. *J. Chem. Eng. Data* **2013**, *58*, 611–624.

(36) Centeno, G.; Sánchez-Reyna, G.; Ancheyta, J.; Muñoz, J. A. D.; Cardona, N. Testing various mixing rules for calculation of viscosity of petroleum blends. *Fuel* **2011**, *90*, 3561–3570.

(37) Amundarain, J.; Chadakowski, M.; Long, B.; Shaw, J. M. Characterization of Physically and Chemically Separated Athabasca Asphaltenes Using Small-Angle Scattering. *Energy Fuels* **2011**, *25* (11), 5100–5122.

(38) Long, B.; Chadakowski, M.; Shaw, J. Impact of Liquid-Vapor to Liquid-Liquid-Vapor Phase Transitions on Asphaltene-Rich Nanoaggregate Behavior in Athabasca Vacuum Residue + Pentane Mixtures. *Energy Fuels* **2013**, *27* (4), 1779–1790.